Miner Deposita (2008) 43:663–675
DOI 10.1007/s00126-008-0184-4

ARTICLE

Atacamite formation by deep saline waters in copper deposits from the Atacama Desert, Chile: evidence from fluid inclusions, groundwater geochemistry, TEM, and ^{36}Cl data

Martin Reich · Carlos Palacios · Miguel A. Parada · Udo Fehn · Eion M. Cameron · Matthew I. Leybourne · Alejandro Zúñiga

Received: 18 December 2007 / Accepted: 13 March 2008 / Published online: 27 May 2008

Abstract The presence of large amounts of atacamite in oxide zones from ore deposits in the Atacama Desert of northern Chile requires saline solutions for its formation and hyperarid climate conditions for its preservation. We investigated the nature and origin of atacamite-forming solutions by means of coupling groundwater geochemical analyses with fluid inclusion data, high-resolution mineralogical observations, and chlorine-36 (^{36}Cl) data in atacamite from the Mantos Blancos and Spence Cu deposits. In both deposits, the salinities of fluid inclusions in atacamite are comparable to those measured in saline groundwaters sampled from drill holes. The average salinity of fluid inclusions in atacamite for the Mantos Blancos and Spence deposits (~7–9 and 2–3 wt.% $NaCl_{eq}$, respectively) are strongly correlated to the salinities at which gypsum supersaturates from groundwaters in both deposits (total dissolved solids ~5–9 and 1–3 wt.% $NaCl_{eq}$, respectively). This correlation is confirmed by transmission electron microscopy observations of atacamite-bearing samples, revealing an intimate association between atacamite and gypsum that can be traced down to the nanometer scale. ^{36}Cl data in atacamite provide new lines of evidence concerning the origin and age of the saline waters that formed atacamite in various stratabound and porphyry Cu deposits from the Atacama Desert. All atacamite samples show very low ^{36}Cl-to-Cl ratios (11×10^{-15} to 28×10^{-15} at at^{-1}), comparable to previously reported ^{36}Cl-to-Cl ratios of deep formation waters and old groundwaters. In addition, ^{36}Cl-to-Cl ratios in atacamite correlate with U and Th concentration in the host rocks but are independent from distance to the ocean. This trend supports an interpretation of the low ^{36}Cl-to-Cl ratios in atacamite as representing subsurface production of fissiogenic ^{36}Cl in secular equilibrium with the solutions involved in atacamite formation. Therefore, ^{36}Cl in atacamite strongly suggest that the chlorine in saline waters related to atacamite formation is old (>1.5 Ma) but that atacamite formation occurred more recently (<1.5 Ma) than suggested in previous interpretations. Our data provide new constraints on the origin of atacamite in Cu deposits from the Atacama Desert and support the recent notion that the formation of atacamite in hyperarid climates such as the Atacama Desert is an ongoing process that has occurred intermittently since the onset of hyperaridity.

Editorial handling: B. Lehmann

M. Reich (✉) · C. Palacios · M. A. Parada
Departamento de Geología,
Facultad de Ciencias Físicas y Matemáticas,
Universidad de Chile,
Santiago, Chile
e-mail: mreich@cec.uchile.cl

U. Fehn
Department of Earth and Environmental Sciences,
University of Rochester,
Rochester, NY 14267, USA

E. M. Cameron
Eion Cameron Geochemical Inc.,
865 Spruce Ridge Road,
Carp, Ontario K0A 1L0, Canada

M. I. Leybourne
Ocean Exploration, GNS Science,
Lower Hutt, New Zealand

A. Zúñiga
Departamento de Ingeniería Mecánica,
Facultad de Ciencias Físicas y Matemáticas,
Universidad de Chile,
Santiago, Chile

Introduction

Atacamite and its polymorph paratacamite ($Cu_2Cl(OH)_3$) are major constituents of supergene oxide zones in many Cu deposits from the Atacama Desert of northern Chile (Sillitoe and McKee 1996; Chávez 2000; Mote et al. 2001; Bouzari and Clark 2002; Hartley and Chong 2002; Dunai et al. 2005; Hartley and Rice 2005; Sillitoe 2005; Rech et al. 2006). Atacamite formation has been traditionally interpreted as a primary product of supergene oxidation (e.g., Chávez 2000), formed after leaching of Cu sulfides by oxygenated meteoric waters that percolated through the deposits. Supergene oxidation of copper porphyry deposits occurred over a long period from 44 to 9 Ma, after which the climate became hyperarid (Arancibia et al. 2006). Atacamite requires saline water for its formation (Hannington 1993), rather than fresh meteoric water. Recognizing this, Arcuri and Brimhall (2003) proposed that atacamite in the Radomiro Tomic deposit, where this is the principal oxide mineral, was formed during supergene oxidation by percolating saline meteoric water. However, atacamite dissolves rapidly or undergoes phase change when exposed to fresh, meteoric water. During the long period prior to the onset of hyperaridity, when oxide zones were exposed to percolating rainwater, any atacamite would have been removed. Moreover, some oxide zones containing atacamite were later covered by piedmont gravels. Stream waters carrying these gravels would have permeated through the oxide zones, removing atacamite. Based on these arguments, Cameron et al. (2007) suggested that atacamite-bearing oxide assemblages are more likely to have formed after the onset of hyperaridity by the replacement of preexisting oxide assemblages, either by earthquake-induced pulses of deep saline waters through the deposits or by meteoric waters which became saline by evaporation at the surface.

When hyperaridity commenced is much debated. Previously, it was thought to have followed the main period of supergene enrichment ending at 14 Ma (Alpers and Brimhall 1988; Sillitoe and McKee 1996). However, recent dating of post-14-Ma supergene events and other evidence (Hartley and Rice 2005; Arancibia et al. 2006) suggest that hyperaridity started as late as 4 Ma. Leybourne and Cameron (2008) provide evidence that atacamite and other secondary Cu minerals may currently be forming by oxidation of hypogene and/or supergene sulfides, suggesting that supergene Cu mineralization is possible even under the hyperarid conditions that dominate the present-day climate of the Atacama Desert.

The aim of this study is to provide further insight into the origin and source of waters that form(ed) atacamite by integrating mineralogical and isotopic data of atacamite with groundwater chemistry data from the Mantos Blancos and Spence Cu deposits in the Atacama Desert of northern Chile. We report salinity data of fluid inclusions trapped in atacamite, and we compare these results with groundwater salinities. In addition, we complement these data with high-resolution transmission electron microscopy (TEM) observations of atacamite samples and ^{36}Cl isotopic data of atacamite from various deposits in the Atacama Desert.

Geologic setting and atacamite occurrence

About 40% of the known Cu resources in the world occur in Chile, and the hyperarid Atacama Desert of northern Chile contains some of the world's largest Cu deposits (Maksaev et al. 2007). Supergene oxidation and leaching processes have produced important enrichment of porphyry and stratabound ("manto-type") Cu deposits, and the economic viability of these deposits is typically dependent on the size and quality of the supergene enrichment blanket that overlies the hypogene Cu–sulfide zones (Sillitoe and McKee 1996; Maksaev et al. 2007). Notable occurrences of atacamite (with variable proportions of other oxide minerals) are found in several Cu deposits in northern Chile. The location of atacamite-bearing deposits, including Mantos Blancos and Spence, is shown on Fig. 1, and the geology of these deposits has been recently reviewed by Ramirez et al. (2006) and Cameron et al. (2007). Both Spence and Mantos Blancos are located along the prominent Antofagasta–Calama Lineament (ACL, Fig. 1), a major structural feature

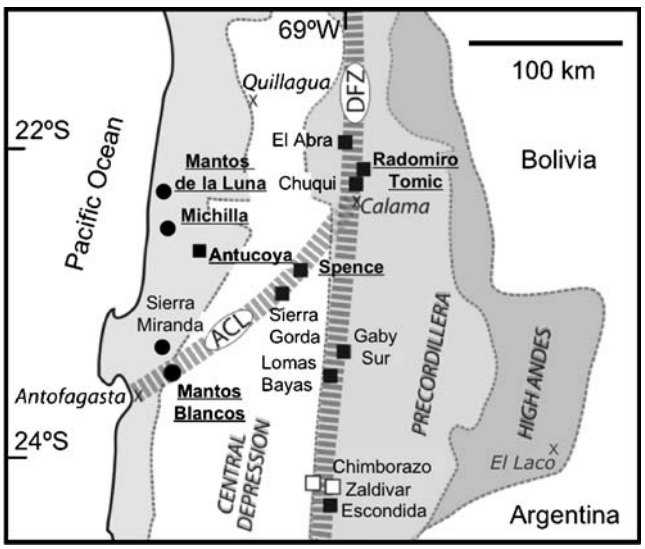

Fig. 1 Map showing the location of various Cu deposits in the Atacama Desert in northern Chile, after Cameron et al. (2007). *Black squares* and *circles* represent atacamite-containing porphyry Cu deposits and other Cu deposits, respectively (*white squares* are other porphyry deposits). Physiographic zones (Coastal Ranges, Central Depression, Precordillera, and High Andes) are depicted in shades of *gray*, and *DFZ* and *ACL* are the Domeyko Fault Zone and the Antofagasta-Calama Lineament (Palacios et al. 2007)

that is thought to have controlled deformation and tectonic rotation in the region since Early Cretaceous (Ramirez et al. 2006). The Spence porphyry Cu deposit contains 231 Mt of sulfide ore at 1.13% Cu and 79 Mt of oxide ore (atacamite and other oxides) at 1.18% Cu (Cameron et al. 2007). Porphyry intrusion and hypogene mineralization (in the porphyries and adjacent andesites) at Spence took place during the Paleocene, at around 57 Ma (Rowland and Clark 2001). The Mantos Blancos porphyry-like deposit also lies on the ACL, and the oxidized ore represents ~30% of the total Cu reserve (200 Mt extracted since 1960; Maksaev et al. 2007). The main ore formation has been related to an Upper Jurassic hydrothermal event at ~140 Ma and consists of hydrothermal breccias, disseminations, and stockworks associated with sodic alteration (Ramirez et al. 2006). Mantos Blancos and Spence deposits are characterized by well-developed atacamite-bearing oxide zones and are covered by ~10–100- and 50–100-m-thick gravels and gypsum-rich saline soil, respectively. The current water tables at the Mantos Blancos and Spence deposits are located at depths of ~400 and 50 to 90 m below the surface, respectively.

Atacamite is the major component of oxide zones of many Cu deposits in the Atacama Desert (Fig. 1). It typically occurs as complex, fine-grained cryptocrystalline aggregates forming veinlets, disseminations and/or replacing preexisting Cu minerals as corrosion coatings, although it occasionally occurs as coarser, millimeter-scale crystals. Atacamite has also been reported as a secondary mineral in the weathered portions of massive sulfide deposits on the modern seafloor (Hannington 1993). Hannington (1993) described atacamite in TAG mounds as occurring in patchy colloform masses, as crystalline aggregates that fill open spaces, and as disseminated crystals intergrown with fine-grained Fe-oxy-hydroxides. The crystalline habits of atacamite include prismatic crystals and equant, rhombic prisms. Individual euhedra range in size from a few tens of micrometers to about 2 mm but are typically less than 500 μm in size (Hannington 1993). Atacamite commonly associates with gypsum in the supergene zones of Cu deposits (e.g., at Radomiro Tomic; Cuadra and Rojas et al. 2001) as well as in submarine hydrothermal ores (Glynn et al. 2006). Sedimentary textures described by Glynn et al. (2006) in supergene alteration zones of submarine hydrothermal sulfides indicate that gypsum and atacamite precipitation may be contemporaneous.

Materials and methods

Groundwater samples collected from drill holes at the Mantos Blancos deposit were analyzed for major and minor cations (Na, K, Ca, Mg, Si, Cu, Fe; inductively coupled plasma optical emission spectrometry) and anions (Cl, SO_4, NO_3; ion chromatography) at Anglo American Laboratories.

Thermometric measurements in primary fluid inclusions trapped in atacamite from the Mantos and Spence deposits were conducted using a Linkam THM-600 stage at the Fluid Inclusions Laboratory, Departamento de Geología, Universidad de Chile. The stage was calibrated with liquid CO_2 inclusions, distilled mercury, and pure water inclusions (accuracy of the melting point temperatures is estimated to be ±0.4°C). Only freezing temperature measurements were performed. Heating experiments to determine the homogenization temperature of the inclusions were avoided, considering the fact that temperatures obtained from heating experiments may be considerably higher than the true values, due to stretching of fluid inclusions trapped in soft minerals such as atacamite (Moh's hardness ~3–3.5). Stretching due to overheating of fluid inclusions in soft minerals (Moh's hardness <3.5) has been extensively documented by many authors, including Bodnar and Bethke (1984), Ulrich and Bodnar (1988), and Vanko and Bach (2005).

Atacamite in oxide zones from ore deposits typically occurs as very fine-grained aggregates in veins and/or disseminated. None of the traditional optical and microanalytical techniques can image the structure and textures of atacamite aggregates below the micrometer level, nor its mineralogical associations at that scale. To investigate the micrometer-to-nanometer texture of fine atacamite aggregates from the Mantos Blancos and Spence deposits, TEM observations were performed at the Laboratorio de Microscopía Electrónica de Transmisión, Departamento de Geología, Universidad de Chile, Santiago, Chile. TEM samples were cut from polished thin sections and final thinning was performed by ion milling with an Ar beam (4.0 keV) in a Gatan precise ion-polishing system. Details on TEM sample preparation are presented elsewhere (Reich et al. 2005). Observation was carried out using a FEI Tecnai F20 FEG TEM operated at 200 kV equipped with an energy-dispersive spectrometry (EDS) detector. Radiation beam damage was not observed during the analyses. Details on the TEM technique can be found in Williams and Carter (1996).

Because of the extremely low abundance of ^{36}Cl in nature, detection of this isotope is only possible by accelerator mass spectrometry (AMS). Isotope determinations of ^{36}Cl in atacamite and water from recent rain events in the area were conducted using AMS at PrimeLab, Purdue University, USA, following the established extraction and analytical methods reported by Fehn et al. (1992) and Sharma et al. (2000). The detection limit is around 1×10^{-15} for the ^{36}Cl-to-Cl ratio with a typical precision of 5–10% (1σ), which decreases, however, considerably for samples close to the detection limit or where carrier material has been used.

Results

Groundwater salinity

The Mantos Blancos groundwaters span a wide range of salinities (Table 1) and can be subdivided into three main groups based on TDS values: (a) low-salinity waters (TDS< 10,000 mg/L), represented by only one sample (14877); (b) saline waters (10,000<TDS<100,000 mg/L, 16 samples); and (c) high-salinity waters (TDS>100,000 mg/L, 15 samples). There is about two orders of magnitude difference in the Cl^- and Na^+ abundance of the three types of waters, as low-salinity waters show values of 2,050 mg/L Cl^- and 1,570 mg/L Na^+, whereas the saline waters and high-salinity waters average 18,376 and 76,251 mg/L Cl^- and 17,779 and 46,223 mg/L Na^+, respectively. Mantos Blancos groundwaters are mainly Na^+–Cl^-–SO_4^{2-}-type waters, and anions are dominated by Cl^-, with all samples showing a strong positive correlation between $Na^+ + Cl^-$ and TDS (Fig. 2a), over the entire range in TDS. A similar trend of increasing SO_4^{2-} with TDS is observed for low-salinity and saline waters, but this correlation breaks down for high-salinity waters, where a strong decrease inSO_4^{2-} with increasing TDS is observed (Fig. 2b). Similar trends have been reported for groundwaters at the Spence deposit by Leybourne and Cameron (2006).

Fluid inclusion salinity

All of the fluid inclusions observed in atacamite from the Spence and Mantos Blancos deposits consist of liquid and vapor (L + V) with no daughter mineral. Most inclusions have diameters of <30 μm, with <30% vapor by volume. Inclusions are scarce and are typically found scattered

Table 1 Major and minor ions of groundwaters from Mantos Blancos deposit, northern Chile

Sample	Cl, mg/L	SO_4, mg/L	NO_3, mg/L	Na, mg/L	K, mg/L	Ca, mg/L	Mg, mg/L	Si, mg/L	Cu, mg/L	Fe, mg/L	pH	TDS, mg/L	TDS[a], wt.%$NaCl_{eq}$
14877	2,050	1,250	0.8	1,570	20	290	20	4.0	1.7	0.7	8.0	6,200	0.36
14253	11,850	8,220	4.6	11,470	70	730	100	8.6	2.1	0.1	7.9	37,900	2.33
14251	11,550	7,680	4.3	11,230	70	700	110	11.3	2.5	0.3	7.9	38,100	2.28
14250	14,100	9,070	4.4	13,440	80	780	130	10.4	2.4	0.2	8.0	42,200	2.75
14249	13,800	9,090	3.6	13,070	80	750	150	11.0	2.4	0.1	7.9	42,400	2.69
14267	12,800	9,800	4.7	12,460	70	690	120	13.9	2.7	0.2	7.5	43,300	2.53
14268	17,000	10,590	4.5	15,960	90	740	200	13.6	2.9	1.9	7.7	52,100	3.30
14270	18,800	12,130	5.1	17,720	90	740	240	14.0	2.2	0.1	7.8	57,400	3.65
14269	23,300	10,410	4.6	18,600	90	860	320	13.9	3.0	0.1	7.6	61,800	4.19
14271	22,700	11,600	4.8	19,470	90	800	310	18.5	5.5	0.3	7.5	62,500	4.22
14751	20,010	14,860	6.9	20,140	160	600	290	18.0	1.5	0.7	7.2	63,000	4.02
14272	19,900	14,870	6.5	20,350	90	670	340	12.8	2.8	0.3	7.5	66,500	4.03
14752	20,480	15,130	7.0	20,540	170	620	310	18.0	1.3	0.7	7.3	66,900	4.10
14755	21,020	15,310	7.3	21,270	170	620	330	19.0	1.7	0.7	7.2	67,000	4.23
14753	20,860	15,190	7.1	21,150	160	620	320	21.0	1.5	0.7	7.3	67,400	4.20
14754	20,790	15,330	7.1	21,380	170	630	320	20.0	1.5	0.7	7.2	67,800	4.22
14952	25,050	25,600	10.0	26,210	260	640	2,290	6.0	1.9	6.7	7.8	93,200	5.13
14894	55,710	4,560	5.9	35,920	620	950	2,070	18.0	0.9	2.8	7.5	110,100	9.16
14252	61,500	1,280	9.7	28,530	130	9,220	1,510	20.1	3.7	1.0	6.9	115,800	9.00
14933	55,950	9,890	7.0	37,200	370	1,140	1,350	4.0	0.4	2.1	7.2	116,100	9.32
13877	55,320	10,000	5.9	38,680	320	1,040	1,030	10.8	0.9	0.8	7.5	116,400	9.40
14285	57,400	1,700	13.5	28,250	100	6,300	1,420	23.1	4.7	3.2	7.3	122,300	8.57
14284	68,300	1,750	12.7	35,710	120	6,180	1,420	15.4	5.4	1.0	6.9	137,900	10.40
14912	69,230	9,680	5.7	48,760	480	1,180	1,980	10.0	0.6	7.5	7.0	138,400	11.80
14876	69,540	10,520	4.6	45,720	290	960	1,700	4.0	2.6	5.1	7.5	138,600	11.53
14936	68,680	10,340	8.7	48,100	460	1,200	1,530	6.0	0.6	4.6	7.3	143,500	11.68
14283	68,400	1,410	12.0	32,860	160	8,000	1,700	19.6	5.0	1.1	6.9	144,000	10.13
14935	76,410	10,430	9.9	51,200	520	1,240	1,770	2.0	0.6	3.9	7.3	155,100	12.76
14932	80,330	10,080	7.5	50,610	500	1,180	2,130	4.0	0.7	2.9	7.3	156,200	13.09
13966	107,500	6,650	5.5	62,950	580	880	2,700	12.5	1.9	2.0	7.3	192,100	17.05
13967	124,000	6,250	6.5	74,050	640	890	3,550	2.0	1.3	2.5	7.0	229,900	19.81
13965	125,500	6,650	6.5	74,800	640	870	3,350	2.0	1.0	2.5	7.0	230,200	20.03

[a] TDS*[weight percent $NaCl_{eq}$]=(Na[milligram per liter] + Cl[milligram per liter])10^{-4}

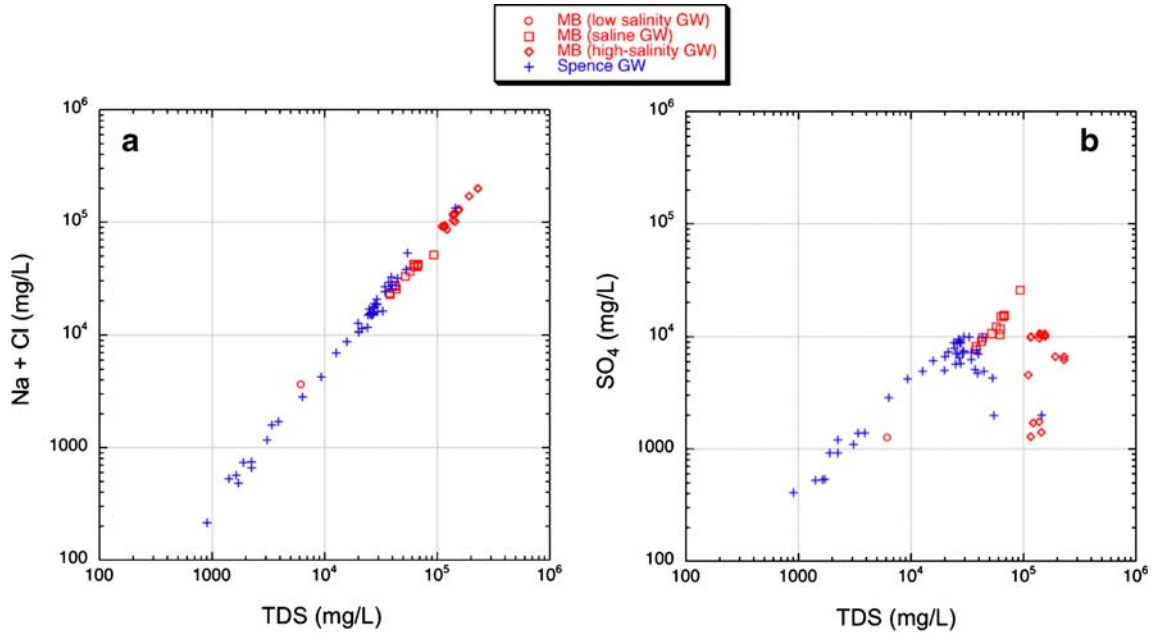

Fig. 2 Plots of total dissolved solids (*TDS*) versus Na + Cl cations (**a**) and SO_4 anions (**b**) for groundwaters from Mantos Blancos and Spence deposits. Data from Spence taken from Leybourne and Cameron (2006)

throughout atacamite crystals, forming clusters (Fig. 3a–d). Due to the scarcity and small size of the inclusions, coupled with the fact that atacamite occurs as polycrystalline aggregates of fine-grained crystals and does not show growth zones under polarized light, the primary or pseudosecondary nature of the inclusions could not be confirmed (secondary inclusions were not observed). The salinity of the fluid inclusions was determined using the formula reported by Bodnar (1993) for the NaCl–H_2O system, as no evidence was observed for either liquid CO_2 or clathrate formation on freezing point depression measurements. Salinities of 48 fluid inclusions trapped within five atacamite samples from Mantos Blancos (each one representing different veinlets) vary between 6.4 and 10.7 wt.% NaCl equivalent ($NaCl_{eq}$, with an average of 8.4 wt.% $NaCl_{eq}$; Fig. 4; Table 2). In contrast, the salinities of 43 fluid

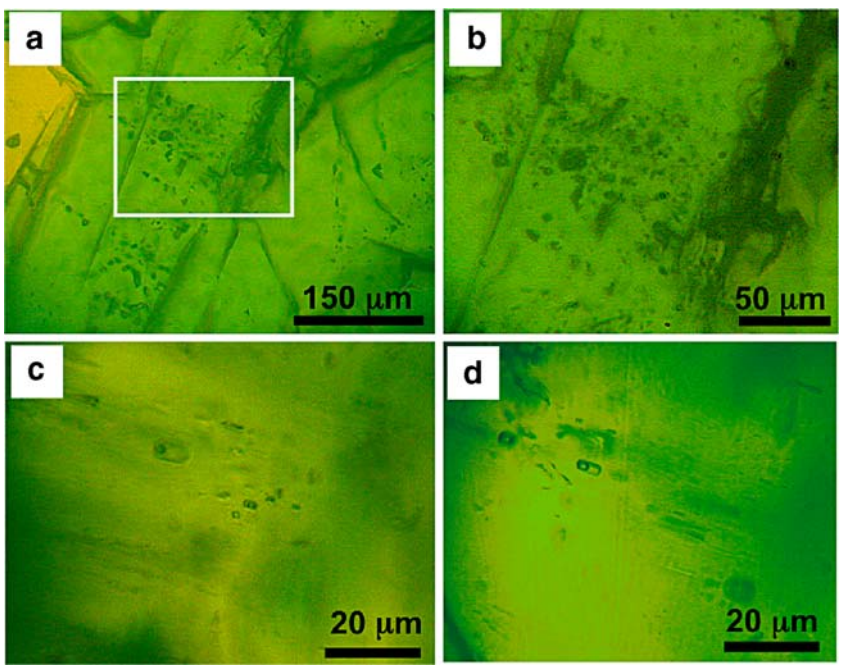

Fig. 3 Photomicrographs of fluid inclusions in atacamite from a Mantos Blancos sample, taken in plane polarized reflected light (uncrossed polars). *Rectangle* in **a** shows magnified area in **b**. All of the fluid inclusions observed in atacamite from Spence and Mantos Blancos deposits (diameters <30 µm, **a**–**d**) consist of liquid and vapor (L + V) with no daughter mineral (**c** and **d**). Inclusions are scarce and are usually found scattered throughout atacamite crystals, forming clusters

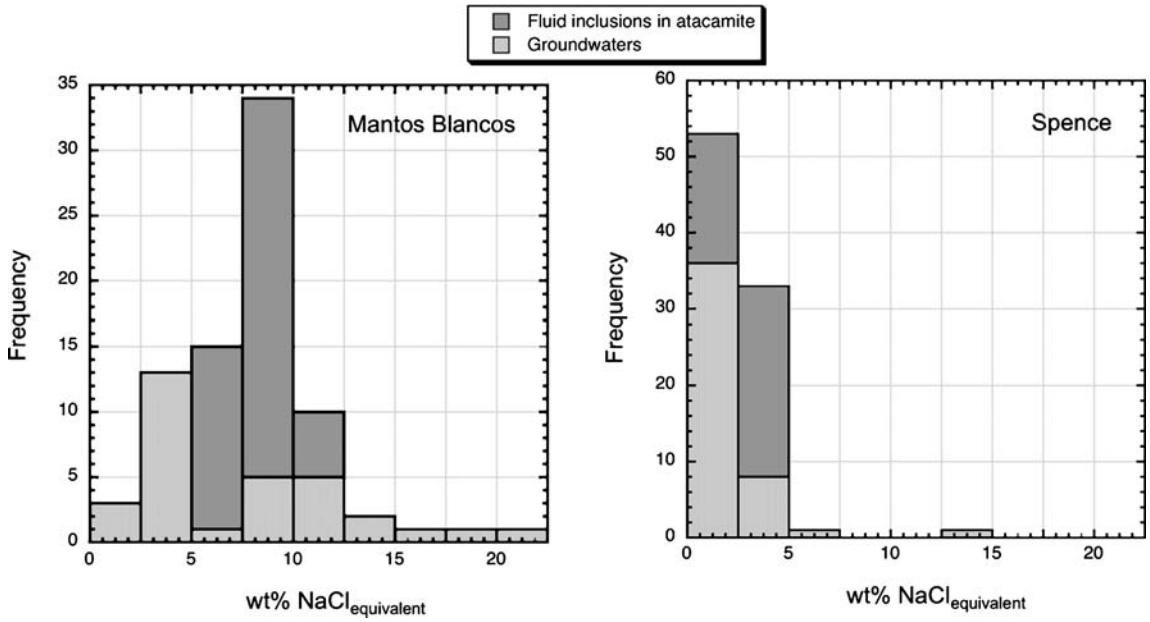

Fig. 4 Histograms showing the distribution of salinities (in wt.% $NaCl_{eq}$) of fluid inclusions in atacamite from Mantos Blancos and Spence deposits in northern Chile

inclusions, determined in seven samples of atacamite-bearing veinlets at Spence, vary between 1.7 and 4.3 wt.% $NaCl_{eq}$, averaging 2.7 wt.% $NaCl_{eq}$ (Fig. 4).

TEM observations

Atacamite occurs as polycrystalline aggregates associated with gypsum in veinlets (Fig. 5a). TEM observations in a selected atacamite–gypsum veinlet sample from the Spence deposit (Fig. 5a) reveal that atacamite is in close association with gypsum at all scales of observation (hand sample to nanoscale, Fig. 5a–e) The presence of atacamite and gypsum at the nanoscale was confirmed using EDS spot analyses. TEM images show dark, opaque, and elongated crystals of atacamite (<10 μm in size) associated with lighter gray, translucent gypsum crystals that show its characteristic cleavage (Fig. 5c). Figure 5d shows a detail of the atacamite–gypsum aggregate microstructure, showing the intergrowth of both minerals, and a layer of gypsum can be seen in the middle of the elongated atacamite grain.

^{36}Cl-to-Cl ratios

In order to gain insight into the origin of the Cl-rich fluids from which atacamite precipitated, the ^{36}Cl contents of nine samples of atacamite from five ore deposits in the Atacama Desert were determined together with two samples from recent rain events (Antofagasta and El Laco). Details of the Michilla (stratabound Cu or Manto-type), Antucoya-Buey Muerto (porphyry Cu), Radomiro Tomic (porphyry Cu), and Mantos de la Luna (manto-type) deposits can be found in Trista-Aguilera et al. (2006), Maksaev et al. (2006, 2007), and Cuadra and Rojas (2001), respectively. This suite of Cu deposits, all characterized by the development of atacamite-bearing oxide zones, covers a geographic range between the Coastal Cordillera near the Pacific Ocean (Mantos Blancos, Mantos de la Luna, Michilla) to the Central Depression (Antucoya-Buey Muerto, Radomiro Tomic and Spence; Fig. 1). Results are reported as the ratio of ^{36}Cl atoms to stable Cl atoms (^{36}Cl to Cl; Table 3). The atacamite samples show low ^{36}Cl-to-Cl ratios, varying from 11×10^{-15} to 28×10^{-15} at at^{-1}. The highest and lowest ^{36}Cl-to-Cl ratios are observed for Mantos Blancos (28×10^{-15}) and Antucoya-Buey Muerto (11×10^{-15}), respectively. In contrast, the two rainwater samples have ^{36}Cl-to-Cl ratios of 867 and 2,247, respectively, a range to be expected for samples from very arid climates and high altitudes (Bentley et al. 1986).

Discussion

Solution salinities, gypsum supersaturation, and the formation of atacamite

A striking feature observed in all atacamite samples analyzed in this study is the close association of atacamite with gypsum. As seen in Fig. 5a–e, atacamite–gypsum aggregates can be traced from a hand-sample scale down to the nanometer range, and the textures observed at all scales suggest that atacamite and gypsum are coeval. Contemporaneous precipitation of gypsum and atacamite has also

Table 2 Fluid inclusion salinity data for atacamite from Mantos Blancos and Spence deposits

Sample	T_m ice (°C)	Salinity, wt.% $NaCl_{equiv}$	Vapor, vol.%	Sample	T_m ice (°C)	Salinity, wt.% $NaCl_{equiv}$	Vapor, vol.%
Mantos Blancos				Spence			
1	−7.1	10.6	10	1	−1.2	2.1	15
	−7.2	10.7	10		−1.4	2.4	15
	−7.0	10.5	20		−1.4	2.4	15
	−7.1	10.6	15		−1.3	2.2	20
2	−6.5	9.9	15		−1.3	2.2	10
	−6.5	9.9	15	2	−2.4	4.0	20
	−6.1	9.3	25		−2.5	4.2	25
	−6.3	9.6	20		−2.5	4.2	10
	−6.8	10.2	15	3	−1.9	3.2	10
	−6.4	9.7	10		−2.1	3.6	20
	−6.2	9.5	10		−2.0	3.4	20
	−6.0	9.2	10		−2.0	3.4	10
	−6.0	9.2	15		−2.6	4.3	15
	−6.2	9.5	15		−2.0	3.4	20
	−6.1	9.3	10	4	−1.7	2.9	25
	−6.6	10.0	10		−1.5	2.6	10
	−6.0	9.2	15		−1.5	2.6	20
3	−4.0	6.4	25		−1.5	2.6	20
	−4.9	7.7	10		−1.6	2.7	30
	−4.2	6.7	15		−1.5	2.6	10
	−4.4	7.0	15		−1.8	3.1	25
	−4.5	7.2	10	5	−1.3	2.2	15
	−4.0	6.4	20		−1.5	2.6	10
	−4.8	7.6	10		−1.2	2.1	10
	−4.2	6.7	10		−1.7	2.9	10
	−4.4	7.0	10		−1.5	2.6	30
	−4.6	7.3	15	6	−1.0	1.7	20
	−4.6	7.3	20		−1.0	1.7	20
	−4.5	7.2	10		−1.0	1.7	15
	−4.4	7.0	10		−1.0	1.7	25
	−4.5	7.2	10		−1.1	1.9	20
	−4.7	7.4	20		−1.1	1.9	25
	−4.5	7.2	15		−1.0	1.7	15
	−4.8	7.6	15		−1.0	1.7	10
4	−5.1	8.0	10		−1.2	2.1	20
	−5.8	9.0	15		−1.1	1.9	25
	−5.4	8.4	15	7	−1.7	2.9	30
	−5.5	8.6	15		−1.9	3.2	10
	−5.9	9.1	10		−1.8	3.1	20
	−5.7	8.8	10		−1.6	2.7	20
	−5.0	7.9	15		−1.8	3.1	20
	−5.2	8.1	15		−1.9	3.2	30
	−5.5	8.6	15		−1.9	3.2	10
	−5.3	8.3	10				
	−5.0	7.9	10				
	−5.2	8.1	10				
	−5.6	8.7	10				
	−5.3	8.3	15				
Summary statistics	n=48; <salinity>±σ=8.4±1.2				n=43; <salinity>±σ=2.7±0.7		

Salinities were calculated using the formula reported by Bodnar (1993).

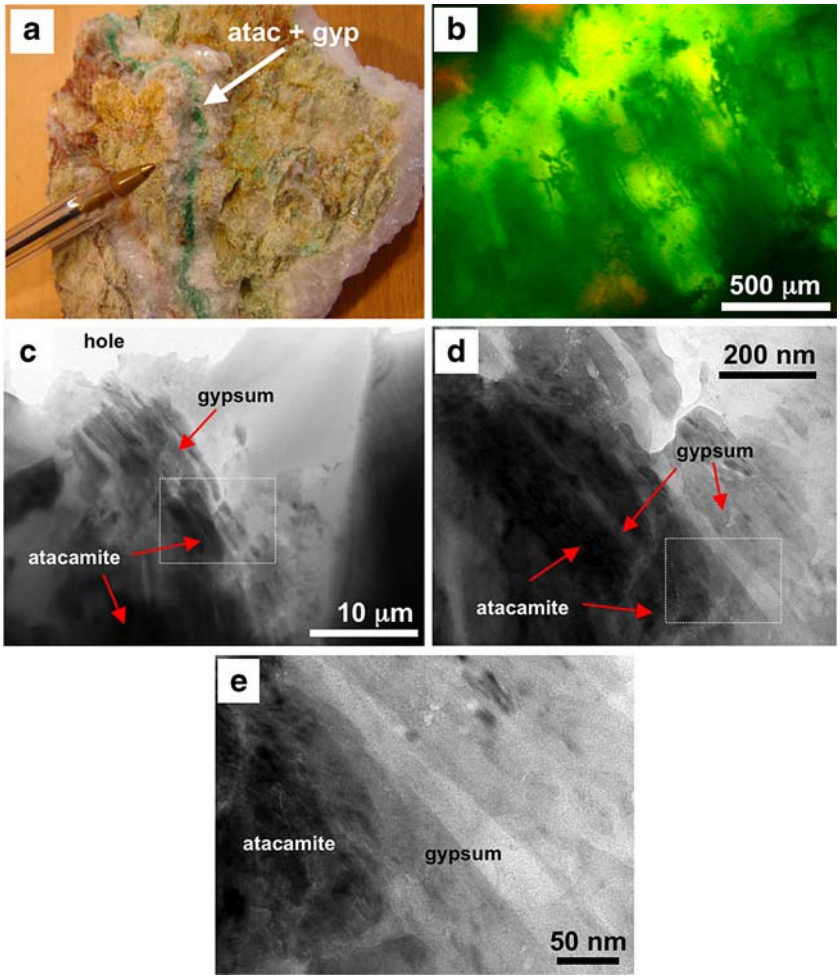

Fig. 5 The atacamite–gypsum association from hand-sample scale down to the nanometer range: **a** atacamite–gypsum veinlet from Spence deposit; **b** photomicrograph of fine-grained aggregates of atacamite in the veinlet shown in **a** (reflected light polarizing microscopy); **c** bright-field TEM images of atacamite aggregates showing a close relation with gypsum at the micron scale. Both minerals were identified by EDS analysis. *Rectangle* shows location of detail in **d**; **d** detail showing the mineralogical association between atacamite and gypsum at the submicrometer range, as seen under TEM observation. Intercalations of gypsum (*lighter*) in atacamite (*darker*) can be observed; **e** magnification of the rectangle area shown in **d**. At the nanometer scale, atacamite and gypsum are found in close association

Table 3 ^{36}Cl-to-Cl ratios in atacamite from ore deposits in the Atacama Desert in northern Chile

Material	Sample	Location	Distance to PO (km)	Elevation (m a.s.l.)	^{36}Cl–Cl ($\times 10^{-15}$ atat^{-1})
Atacamite					
Mantos de la Luna	ML-c	70° 13′ W/22° 20′ S	0.5	1,000	15.3±3.6
Mantos de la Luna	ML-c-a	70° 13′ W/22° 20′ S	0.5	1,000	16.6±4.1
Mantos de la Luna	ML-c-b	70° 13′ W/22° 20′ S	0.5	1,000	14.3±2.3
Michilla	SS-b	70° 07′ W/22° 51′ S	13	1,100	19.9±2.9
Antucoya	AB-b	70° 41′ W/22° 37′ S	35	1,700	11.1±1.7
Mantos Blancos	MB-b	70° 06′ W/23° 22′ S	40	1,100	26.5±5.7
Mantos Blancos	MB-b-a	70° 06′ W/23° 22′ S	40	1,100	28.0±4.4
Spence	SP-b	69° 18′ W/22° 48′ S	100	1,600	13.2±2.3
Radomiro Tomic	RT-a	60° 01′ W/22° 28′ S	150	2,950	16.1±1.9
Rainwater					
Antofagasta; March 18, 2006	RWA-a	70° 22′ W/23° 40′ S	0.5	50	867±167
El Laco; January 27, 2007	El Laco	67° 30′ W/23° 42′ S	210	4,850	2,247±315

The two rainwater samples were prepared using carrier.
PO Pacific Ocean

been reported by Glynn et al. (2006) in supergene alteration of submarine hydrothermal sulfides.

Present-day groundwater salinity (TDS) and sulfate (SO_4^{2-}) trends (Fig. 2b) and fluid inclusion salinities in atacamite (Fig. 4) provide additional insights into this mineralogical association. At the Mantos Blancos and Spence deposits, the decrease in SO_4^{2-} of the groundwaters at the highest salinities (Fig. 2b) suggests that SO_4^{2-} concentrations are controlled, in part, by the formation of gypsum (Leybourne and Cameron 2006). Therefore, these highest TDS values reflect the salinities at which gypsum supersaturated from groundwaters, ~100,000 and ~30,000 mg/L for Mantos Blancos and Spence, respectively. This argument is supported by mineral saturation calculations reported by Leybourne and Cameron (2006, 2008). In the cited studies, determination of mineral saturation indices for groundwaters at Spence reveal that the highest salinity waters (west of the deposit) are supersaturated with respect to gypsum and close to (or exceeding) saturation with respect to secondary minerals such as atacamite.

In order to make the salinities of the Na–Cl–SO_4-rich groundwaters from Mantos Blancos and Spence (expressed as TDS in milligram per liter) comparable to the salinities of fluid inclusions trapped in atacamite from both deposits (expressed as weight percent $NaCl_{eq}$), TDS values of groundwaters have been converted to weight percent $NaCl_{eq}$ according to TDS*[weight percent $NaCl_{eq}$]=(Na[milligram per liter] + Cl[milligram per liter])10^{-4}. When the gypsum-saturation salinities of groundwaters are compared with the fluid inclusion salinity data in atacamite for both deposits in a single diagram (Fig. 6), a striking correlation arises. The average salinities of fluid inclusions in atacamite for Mantos Blancos and Spence deposits (~7–9 and 2–3 wt.% $NaCl_{eq}$, respectively, Fig. 6, vertical lines) are strongly correlated to the salinities at which gypsum precipitates from groundwaters in both deposits (corrected TDS* ~5–9 and 1–3 wt.% $NaCl_{eq}$, respectively, Fig. 6, trend line inflections). Therefore, as a first approximation, this correlation suggests that the range of salinities from which atacamite–gypsum formed is comparable to present-day, highly-saline gypsum- (and atacamite)-saturated groundwaters.

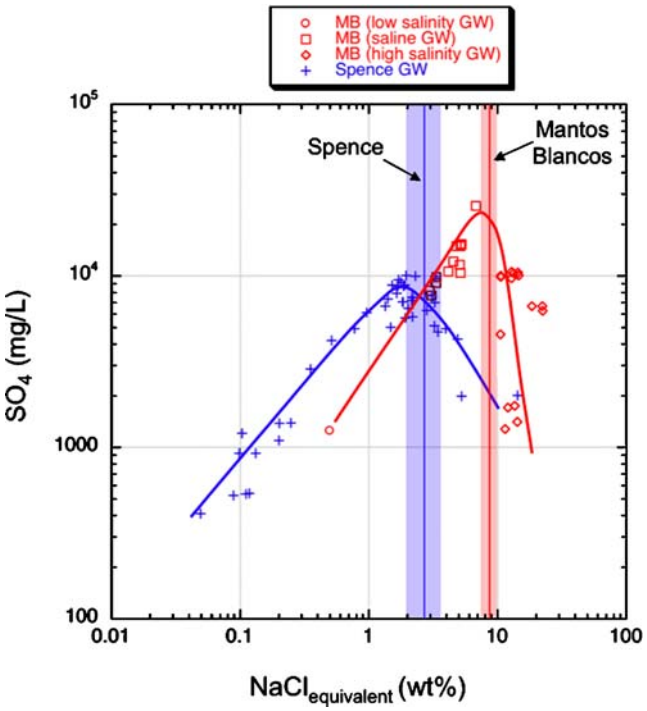

Fig. 6 Sulfate content (SO_4, milligram per liter) versus salinity (weight percent $NaCl_{eq}$, as calculated from TDS data, see text for detail) of groundwaters from Mantos Blancos and Spence. The salinity at which groundwaters supersaturate with respect to gypsum (inflection points) correlate well with the salinity range of fluid inclusions in atacamite from the same deposits (shown as *shaded vertical intervals* defined by the average (*center line*)±standard deviation of salinities from Table 2)

A deep, old, and saline source for atacamite formation

Although it has long been recognized that saline waters can form by evaporation of groundwaters of meteoric origin in hyperarid climates, recent studies report evidence of alternative sources for the Cl-rich solutions required to form atacamite. Cameron et al. (2002, 2007) propose that deep saline formation waters (basinal brines), dewatered from sedimentary rocks underlying the Atacama Desert, can be forced to surface by tectonic pumping during earthquakes. This hypothesis is supported by different lines of evidence, including: (a) the development of geochemical anomalies in salt soils over orebodies that are strongly correlated with the distribution of fractures–faults below (Cameron et al. 2002; Palacios et al. 2005); (b) stable isotopic signatures that confirm involvement of seawater-like, deep formation waters–basinal brines that mix to variable degrees with the less saline, regional groundwater flow (e.g., $\delta^{37}Cl$ in atacamite at Radomiro Tomic, Arcuri and Brimhall 2003; δD and $\delta^{18}O$ in groundwaters at Spence, Leybourne and Cameron 2006).

The first measurements of ^{36}Cl in atacamite, presented here, provide new lines of evidence concerning the origin of the saline waters that formed atacamite (Table 3). Natural ^{36}Cl can be derived from cosmogenic, fissiogenic, and anthropogenic sources (Fehn et al. 1988; Snyder at al. 2003; Fehn and Snyder 2005). The anthropogenic component is related to thermonuclear weapons tests, and considering the fact that atmospheric ^{36}Cl has returned to prebomb ratios since about 1980 (Suter et al. 1987) we will focus on the other two sources. The cosmogenic component is formed by spallation by cosmic rays of Ar in the atmosphere and Ca and K in surface rocks and has been

used to determine groundwater ages and exposure ages of surface rocks (Purdy et al. 1996; Phillips et al. 2003). In theory, the subsurface isolation time of water between 5×10^4 and 2×10^6 years can be determined using this method, considering that the half-life of ^{36}Cl is 0.3 Ma (Fehn and Snyder 2005). On the other hand, the fissiogenic component is a result of capture by ^{35}Cl (e.g., in pore waters) of neutrons produced by the decay of U and Th isotopes (e.g., in the host rocks). The buildup of ^{36}Cl is a function of time, concentration of U and Th, and the presence of neutron-absorbing atoms competing with ^{35}Cl. The presence of fissiogenic ^{36}Cl can be used to determine potential sources for fluids (Rao et al. 1996) or the residence time of fluids in a given formation if the neutron flux can be estimated (Fehn et al. 1992; Fehn and Snyder 2005).

Despite the low ^{36}Cl contents measured in atacamite in our samples (^{36}Cl–Cl ~$(11–28)\times10^{-15}$, Table 3), its detection suggests that ^{36}Cl was inherited from the waters from which atacamite formed. Thus, the data can be potentially used as an isotopic tracer for the waters involved in the genesis of atacamite if the main source(s) component(s) for ^{36}Cl can be sorted out and assuming that the ^{36}Cl budget incorporated in atacamite (cosmogenic or fissiogenic in origin) represents the ^{36}Cl budget of the water from which it precipitated (assuming, in this particular case, no fluid–mineral isotope fractionation and/or ^{36}Cl loss or addition after the formation of atacamite).

All atacamite samples show very low ^{36}Cl-to-Cl ratios, close to the AMS detection limit of 1×10^{-15}, comparable to previously reported ^{36}Cl/Cl ratios of deep formation waters and old groundwaters. Low ^{36}Cl-to-Cl ratios, interpreted as in secular equilibrium with in situ (fissiogenic) ^{36}Cl, have been reported in ultradeep mine waters at the Witwatersrand Basin in South Africa (Lippmann et al. 2003), deep groundwaters from the Great Artesian Basin in Australia (Lehmann et al. 2003), waters from the German Continental Deep Drill Hole in Northern Bavaria (Fehn and Snyder 2005), deep formation waters from the Fruitland Formation in Colorado and New Mexico (Snyder et al. 2003; Snyder and Fabryka-Martin 2007), deep groundwater from the Northern Sahara (Guendouz and Michelot 2006), and the East Irish Sea Basin (Metcalfe et al. 2007). In all these cases, low ^{36}Cl-to-Cl ratios ($<30\times10^{-15}$) reflect subsurface, fissiogenic production of ^{36}Cl in secular equilibrium indicating an age in excess of 1.5 Ma, or five times the half-life of ^{36}Cl. Although the meteoric component cannot be discarded, disentangling the cosmogenic (meteoric) ^{36}Cl signal is typically difficult, in particular for deeper and more saline groundwater, mainly due to subsurface production of ^{36}Cl by neutron capture of ^{35}Cl and transport from adjacent aquifers or pore water reservoirs (Lehmann et al. 2003).

A potential check on the dominant source of chlorine in these deposits is possible by relating the results to the distance from the ocean and altitude. ^{36}Cl-to-Cl ratios in rainwater and resulting surface or groundwaters show a strong dependence on the distance from the ocean because chlorine in the atmosphere is derived predominantly from sea spray. The long residence time of chlorine in the oceans results in marine ^{36}Cl-to-Cl ratios below 0.5×10^{-15} (i.e., below the detection limit of AMS). In the atmosphere, ^{36}Cl-to-Cl ratios increase with altitude because the production rate of ^{36}Cl diminishes as cosmic rays are attenuated passing through the atmosphere. As a result of these processes, ^{36}Cl-to-Cl ratios in surface waters generally increase strongly with distance from the oceans and with altitude (e.g., Bentley et al. 1986), also observed for the two rainwater samples measured for this study. In contrast to these surface water samples, results for the atacamite samples do not show a correlation with distance from the oceans or altitude, suggesting that ^{36}Cl in these deposits is mainly derived not from cosmogenic but from fissiogenic sources.

In order to further evaluate the role of fissiogenic ^{36}Cl as a potential source for ^{36}Cl in atacamite, we related the abundances of U and Th in the host rocks of each ore deposit (reported by Dietrich 1999; Oliveros 2005; Ramírez et al. 2008) to their respective ^{36}Cl-to-Cl ratios in atacamite (Fig. 7). There is a positive correlation between U + Th concentration in the host rocks and ^{36}Cl-to-Cl ratios in atacamite, with the highest ^{36}Cl–Cl values at Mantos Blancos and the lowest at Antucoya and Spence. This trend supports our interpretation of the low ^{36}Cl-to-Cl ratios in atacamite ($11–28\times10^{-15}$ at at^{-1}) as representing subsurface production of fissiogenic ^{36}Cl in secular equilibrium with the solutions involved in the atacamite origin (Lehmann et al. 2003; Lippmann et al. 2003). Because atacamite does not contain U or Th itself, the production of ^{36}Cl is no longer supported once chlorine has entered the minerals and the ^{36}Cl-to-Cl ratio starts to decrease with age. The fact that we still found measurable ^{36}Cl in atacamite indicates then that the formation of these minerals was relatively recent. The ^{36}Cl data strongly suggest that the chlorine in the saline waters related to atacamite formation is old in origin (>1.5 Ma) but that the atacamite formation occurred less than 1.5 Ma ago (or 5× half-life of ^{36}Cl).

Although more than one mechanism may be involved in formation of atacamite in the hyperarid Atacama Desert, the results support the tectonic pumping model proposed by Cameron et al. (2002, 2007). In the context of this model, saline formation water from the dewatering of the sedimentary basin is carried up through the deposit, modifying the existing oxide assemblage, creating an atacamite-stable assemblage. During earthquakes, the saline water is forced to the surface of the covering gravels, creating saline anomalies plus Cu derived from the deposit. Palacios et al. (2005) reported Cu anomalies in soils above the Mantos Blancos copper deposit. Although the Cu anomalies in

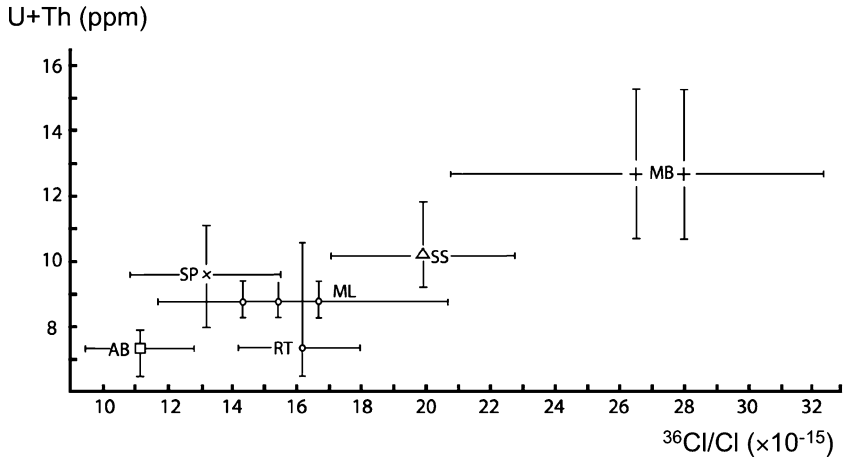

Fig. 7 Variation of ^{36}Cl-to-Cl ratios in atacamite as a function of the U + Th concentration of host rocks, for various deposits in the Atacama Desert in northern Chile. *AB* = Antucoya-Buey Muerto, *SP* = Spence, *ML* = Mantos de la Luna, *RT* = Radomiro Tomic, *SS* = Michilla, and *MB* = Mantos Blancos

surface salt samples (gypsum + anhydrite + halite) over the ore bodies are spiky, their contrast with the background Cu values is remarkable. The same study reports a good correlation between Cu and Na where the concentration of Cu is high and shows that Cu anomalies spatially correlate with faults that crosscut Cu mineralization. The previous observation is confirmed by the presence of salt efflorescences (halite + gypsum) that contain atacamite and chalcanthite at the surface along major active faults near the deposits (e.g., Salar del Carmen fault close to the Mantos Blancos), strongly suggesting that Cu was brought to the surface by saline waters. Copper anomalies from Miocene alluvial gravel soils above the Spence porphyry copper have also been reported by Cameron and Leybourne (2005). The anomalous Cu values developed over the ore deposit show the same spiky response documented by Palacios et al. (2005), and the peaks are observed in zones where the partly salt-cemented gravels are fractured. Enzyme leach and deionized water analyses, which measure water-soluble constituents, evidence Cl and Na anomalies in gravel soils above the Spence deposit and also over fractured zones (Cameron et al. 2002; Cameron and Leybourne 2005). These fracture zones over the deposit are interpreted to represent seismically active basement faults that have propagated through the gravel cover Cameron and Leybourne (2005), suggesting an important relationship between the ascent of saline, deep, and old waters and atacamite formation in hyperarid regions such as the Atacama Desert.

Summary and conclusions

The formation of atacamite in oxide zones in Cu deposits from the Atacama Desert in northern Chile is related to gypsum-saturated saline groundwaters (TDS*>20,000 mg/L or 2 wt.% $NaCl_{eq}$), as confirmed by fluid inclusions in atacamite and present-day groundwater chemistry. The salinity at which groundwaters at the Spence and Mantos Blancos saturate with respect to gypsum (1–3 and 5–9 wt.% $NaCl_{eq}$, respectively) is in the range of salinities measured in fluid inclusions in atacamite, suggesting a close connection between gypsum saturation and atacamite formation. This genetic link is confirmed by observations at different scales that confirm a close mineralogical association between these two minerals, from sample scale down to the nanometer range. In addition, ^{36}Cl data in atacamite show that the low but detectable ^{36}Cl/Cl ratios measured in atacamite ($11–28\times10^{-15}$ atat^{-1}) are probably related to fissiogenic production in the subsurface, suggesting that atacamite in these deposits is produced from chloride in saline waters with ages in excess of 1.5 Ma but that the formation process itself occurred relatively recently (<1.5 Ma).

These results, coupled with previous studies of groundwater chemistry and stable isotope distributions, suggest a deep origin for the saline waters responsible for the formation of atacamite. Our results provide new constraints on the age of atacamite in ore deposits from the Atacama

Fig. 8 Atacamite in miner boots recovered from a deep gallery (150 m deep) in early 1900s workings around the late Paleocene Sierra Gorda Cu-porphyry deposit (photo courtesy of the Geology Museum of the Department of Geosciences, Universidad Católica del Norte, UCN, Antofagasta, Chile). Atacamite (*green*) was confirmed by powder X-ray diffraction analysis at UCN

Desert and support the recent notion that supergene enrichment may have occurred more recently (<1.5 Ma) than many models for the climate of northern Chile suggest (e.g., 9–14 Ma, Alpers and Brimhall 1988; 3–6 Ma, Hartley and Rice 2005). The results suggest that formation of atacamite in hyperarid climates such as the Atacama Desert is an ongoing process (e.g., Fig. 8) that has occurred intermittently, since the onset of hyperaridity.

Acknowledgements Support for this study was received from Comisión Nacional de Ciencia y Tecnología de Chile grant # 1070736 to Carlos Palacios, Martin Reich, and Miguel Angel Parada. We are grateful to BHP-Billiton for logistical assistance and for providing access to the Spence deposit and specifically to Martin J. Williams, Mario Sáez, Walter Ruf, and Jorge Peña for their help during open-pit and core sampling. We also thank Anglo American for providing us with samples from Mantos Blancos and for releasing analytical data for publication (research contract D-1012). The transmission electron microscope used in this work was acquired under the Mecesup grant UCH-0205. We thank Christian Nievas and Marcela Robles for TEM sample preparation. Z. Lu at the University of Rochester prepared the AgCl targets; M. Caffee and the AMS group at PrimeLab, Purdue University, carried out the ^{36}Cl determinations; we appreciate their efforts. We acknowledge Bernd Lehmann for his helpful and constructive review of the manuscript.

References

Alpers CN, Brimhall GH (1988) Middle Miocene climatic change in the Atacama Desert, northern Chile: evidence from supergene mineralization at La Escondida. Geol Soc Am Bull 100:1640–1656

Arancibia G, Matthews SJ, De Arce CP (2006) K-Ar and Ar-40/Ar-39 geochronology of supergene processes in the Atacama Desert, Northern Chile: tectonic and climatic relations. J Geol Soc London 163:107–118

Arcuri T, Brimhall G (2003) The chloride source for atacamite mineralization at the Radomiro Tomic porphyry copper deposit, Northern Chile. Econ Geol 98:1667–1681

Bentley HW, Phillips FM, Davis SN (1986) Chlorine-36 in the terrestrial environment. In: Fritz P, Fontes JC (eds) Handbook of environmental isotopes, vol. 2(B). The terrestrial environment. Elsevier, Amsterdam, pp 420–480

Bodnar RJ (1993) Revised equation and table for determining the freezing-point depression of H_2O–NaCl solutions. Geochim Cosmochim Acta 57:683–684

Bodnar RJ, Bethke PM (1984) Systematics of stretching of fluid inclusions I: fluorite and sphalerite at an atmosphere confining pressure. Econ Geol 79:141–161

Bouzari F, Clark AH (2002) Anatomy, evolution, and metallogenic significance of the supergene orebody of the Cerro Colorado porphyry copper deposit, I region, northern Chile. Econ Geol 97:1701–1740

Cameron EM, Leybourne MI (2005) Relationship between groundwater chemistry and soil geochemical anomalies at the Spence copper porphyry deposit, Chile. Geochem Explor Environm Analysis A 5:135–145

Cameron EM, Leybourne MI, Kelley DL (2002) Exploring for deeply covered mineral deposits: formation of geochemical anomalies in northern Chile by earthquake-induced surface flooding of mineralized groundwaters. Geology 30:1007–1010

Cameron EM, Leybourne MI, Palacios C (2007) Atacamite in the oxide zone of copper deposits in northern Chile: involvement of deep formation waters? Miner Deposita 42:205–218

Chávez WX (2000) Supergene oxidation of copper deposits: zoning and distribution of copper oxide minerals. Soc Econ Geol News 41:1–21

Cuadra P, Rojas G (2001) Oxide mineralization at the Radomiro Tomic porphyry copper deposit, northern Chile. Econ Geol 96: 387–400

Dietrich A (1999) Metallogenie, Geochemie und Schmelzeinschluss-Untersuchungen von tin porphyry und copper porphyry-Lagerstatten der zentralen Anden (Bolivien, Chile). Ph.D. Thesis, Clausthal University, Germany, 198 pp

Dunai TJ, González-Lopez GA, Juez-Larre J (2005) Oligocene–Miocene age of aridity in the Atacama Desert revealed by exposure dating of erosion-sensitive landforms. Geology 33:321–324

Fehn U, Snyder GT (2005) Residence times and source ages of deep crustal fluids: interpretation of l-129 and Cl-36 results from the KTB-VB drill site, Germany. Geofluids 5:42–51

Fehn U, Rich B, Tullai S, Kubik PW, Elmore D, Teng R (1988) Determination of Cl-36 and I-129 in waters from Cherry Hill, CA, a gold-bearing geothermal system. Chem Geol 70:135–135

Fehn U, Peters EK, Tullai-Fitzpatrick S, Kubik PW, Sharma P, Teng RTD, Gove HE, Elmore D (1992) I-129 and Cl-36 concentrations in waters of the Eastern Clear Lake Area, California: residence times and source ages of hydrothermal fluids. Geochim Cosmochim Acta 56:2069–2079

Glynn S, Mills RA, Palmer MR, Pancost RD, Severmann S, Boyce AJ (2006) The role of prokaryotes in supergene alteration of submarine hydrothermal sulfides. Earth Planet Sci Lett 244: 170–185

Guendouz A, Michelot JL (2006) Chlorine-36 dating of deep groundwater from northern Sahara. J Hydrol 328:572–580

Hannington M (1993) The formation of atacamite during weathering of sulfides on the modern seafloor. Can Mineral 31:945–956

Hartley AJ, Chong G (2002) Late Pliocene age for the Atacama Desert: implications for the desertification of western South America. Geology 30:43–46

Hartley AJ, Rice CM (2005) Controls on supergene enrichment of porphyry copper deposits in the Central Andes: a review and discussion. Miner Deposita 40:515–525

Lehmann BE, Love A, Purtschert R, Collon P, Loosli HH, Kutschera W, Beyerle U, Aeschbach-Hertig W, Kipfer R, Frape SK, Herczeg A, Moran J, Tolstikhin IN, Groning M (2003) A comparison of groundwater dating with Kr-81, Cl-36 and He-4 in four wells of the Great Artesian Basin, Australia. Earth Planet Sc Lett 211:237–250

Leybourne MI, Cameron EM (2006) Composition of groundwaters associated with porphyry-Cu deposits, Atacama Desert, Chile: elemental and isotopic constraints on water sources and water–rock reactions. Geochim Cosmochim Acta 70:1616–1635

Leybourne MI, Cameron EM (2008) Source, transport, and fate of rhenium, selenium, molybdenum, arsenic, and copper in groundwater associated with porphyry-Cu deposits, Atacama Desert, Chile. Chem Geol 247:208–228

Lippmann J, Stute M, Torgersen T, Moser DP, Hall JA, Lin L, Borcsik M, Bellamy RES, Onstott TC (2003) Dating ultra-deep mine waters with noble gases and Cl-36, Witwatersrand Basin, South Africa. Geochim Cosmochim Acta 67:4597–4619

Luo SD, Ku TL (1991) U-series isochron dating: a generalized method employing total sample dissolution. Geochim Cosmochim Acta 55:555–564

Maksaev V, Munizaga F, Fanning M, Palacios C, Tapia J (2006) SHRIMP U-Pb dating of the Antucoya porphyry copper deposit:

new evidence for an Early Cretaceous porphyry-related metallogenic epoch in the Coastal Cordillera of northern Chile. Miner Deposita 41:637–644

Maksaev V, Townley B, Palacios C, Camus F (2007) Metallic ore deposits. In: Moreno T, Gibbons W (eds) The geology of Chile. The Geological Society, London, pp 179–199

Metcalfe R, Crawford MB, Bath AH, Littleboy AK, Degnan PJ, Richards HG (2007) Characteristics of deep groundwater flow in a basin marginal setting at Sellafield, Northwest England: Cl-36 and halide evidence. Appl Geochem 22:128–151

Mote TI, Brimhall GH, Tidy-Finch E, Muller G, Carrasco P (2001) Application of mass-balance modeling of sources, pathways, and sinks of supergene enrichment to exploration and discovery of the Quebrada Turquesa exotic copper orebody, El Salvador district, Chile. Econ Geol 96:367–386

Oliveros V (2005) Etude géochronologique des unités magmatiques Jurassiques et Crétacé inférieur du nord du Chili (18°30′ - 24°S, 60° 30 - 70°30′W): origine, mise en Place, altération, métamorphisme et minéralisations associées. Ph.D. Thesis, Université de Nice-Antipolis, France, 285 pp

Palacios C, Guerra N, Townley B, Lahsen A, Parada M (2005) Copper geochemistry in salt from evaporite soils, coastal range of the Atacama Desert, northern Chile: an exploration tool for blind Cu deposits. Geochem Explor Environm Analysis A 5:371–378

Palacios C, Ramirez LE, Townley B, Solari M, Guerra N (2007) The role of the Antofagasta–Calama Lineament in ore deposit deformation in the Andes of northern Chile. Miner Deposita 42:301–308

Phillips FM, Ayarbe JP, Harrison JBJ, Elmore D (2003) Dating rupture events on alluvial fault scarps using cosmogenic nuclides and scarp morphology. Earth Planet Sc Lett 215:203–218

Purdy CB, Helz GR, Mignerey AC, Kubik PW, Elmore D, Sharma P, Hemmick T (1996) Aquia aquifer dissolved Cl- and Cl-36/Cl: implications for flow velocities. Water Resour Res 32:1163–1171

Ramirez LE, Palacios C, Townley B, Parada MA, Sial AN, Fernandez-Turiel JL, Gimeno D, Garcia-Valles M, Lehmann B (2006) The Mantos Blancos copper deposit: An Upper Jurassic breccia-style hydrothermal system in the coastal range of northern Chile. Miner Deposita 41:246–258

Ramírez LE, Parada MA, Palacios C, Wittenbrink J (2008) Magmatic evolution of the Mantos Blancos copper deposit, Coastal Range of northern Chile: insight from Sr-Nd isotope, geochemical data and silicate melt inclusions. Resour Geol 58:124–142

Rao U, Fehn U, Teng RTD, Goff F (1996) Sources of chloride in hydrothermal fluids from the Valles caldera, New Mexico: a Cl-36 study. J Volcanol Geoth Res 72:59–70

Rech JA, Currie BS, Michalski G, Cowan AM (2006) Neogene climate change and uplift in the Atacama Desert, Chile. Geology 34:761–764

Reich M, Kesler SE, Utsunomiya S, Palenik CS, Chryssoulis SL, Ewing RC (2005) Solubility of gold in arsenian pyrite. Geochim Cosmochim Acta 69:2781–2796

Rowland MD, Clark AH (2001) Temporal overlap of supergene alteration and high-sulphidation mineralization in the Spence porphyry copper deposit, II Region, Chile. In: Geological Society of America Annual Meeting, Boston, Abstract 28064

Sharma P, Bourgeois M, Elmore D, Granger D, Lipschutz ME, Ma X, Miller T, Mueller K, Rickey F, Simms P, Vogt S (2000) PRIME lab AMS performance, upgrades and research applications. Nucl Instrum Meth B 172:112–123

Sillitoe RH (2005) Supergene oxidized and enriched porphyry copper and related deposits. In: Hedenquist JW, Thompson JFH, Goldfarb RJ, Richards JP (eds) Economic Geology 100th Anniversary Volume. Society of Economic Geologists, Littleton, pp 723–768

Sillitoe RH, McKee EH (1996) Age of supergene oxidation and enrichment in the Chilean porphyry copper province. Econ Geol 91:164–179

Snyder GT, Fabryka-Martin JT (2007) I-129 and Cl-36 in dilute hydrocarbon waters: marine-cosmogenic, in situ, and anthropogenic sources. Appl Geochem 22:692–714

Snyder GT, Riese WC, Franks S, Fehn U, Pelzmann WL, Gorody AW, Moran JE (2003) Origin and history of waters associated with coalbed methane: I-129, Cl-36, and stable isotope results from the Fruitland Formation, CO and NM. Geochim Cosmochim Acta 67:4529–4544

Suter M, Beer J, Bonani G, Hofmann HJ, Michel D, Oeschger H, Synal HA, Wölfli W (1987) Cl-36 studies at the ETH SIN-AMS Facility. Nucl Instrum Meth B 29:203–206

Trista-Aguilera D, Barra F, Ruiz J, Morata D, Talavera-Mendoza O, Kojima S, Ferraris F (2006) Re-Os isotope systematics for the Lince-Estefania deposit: constraints on the timing and source of copper mineralization in a stratabound copper deposit, Coastal Cordillera of Northern Chile. Miner Deposita 41:99–105

Ulrich MR, Bodnar RJ (1988) Systematics of stretching of fluid inclusions.2. Barite at 1-atm confining pressure. Econ Geol 83: 1037–1046

Vanko DA, Bach W (2005) Heating and freezing experiments on aqueous fluid inclusions in anhydrite: recognition and effects of stretching and the low-temperature formation of gypsum. Chem Geol 223:35–45

Williams DB, Carter CB (1996) Transmission electron microscopy, 1–4. Plenum Press, New York